

Report Documentation Page

Form Approved
OMB No. 0704-0188

Public reporting burden for the collection of information is estimated to average 1 hour per response, including the time for reviewing instructions, searching existing data sources, gathering and maintaining the data needed, and completing and reviewing the collection of information. Send comments regarding this burden estimate or any other aspect of this collection of information, including suggestions for reducing this burden, to Washington Headquarters Services, Directorate for Information Operations and Reports, 1215 Jefferson Davis Highway, Suite 1204, Arlington VA 22202-4302. Respondents should be aware that notwithstanding any other provision of law, no person shall be subject to a penalty for failing to comply with a collection of information if it does not display a currently valid OMB control number.

1. REPORT DATE 05 DEC 2007		2. REPORT TYPE		3. DATES COVERED 00-00-2007 to 00-00-2007	
4. TITLE AND SUBTITLE The Kelvin Wave and the Madden-Julian Oscillation in Aqua-plant Simulations by the Naval Research Laboratory Spectral Element Atmospheric Model (NSEAM)				5a. CONTRACT NUMBER	
				5b. GRANT NUMBER	
				5c. PROGRAM ELEMENT NUMBER	
6. AUTHOR(S)				5d. PROJECT NUMBER	
				5e. TASK NUMBER	
				5f. WORK UNIT NUMBER	
7. PERFORMING ORGANIZATION NAME(S) AND ADDRESS(ES) Naval Research Laboratory, Monterey, CA, 93943				8. PERFORMING ORGANIZATION REPORT NUMBER	
9. SPONSORING/MONITORING AGENCY NAME(S) AND ADDRESS(ES)				10. SPONSOR/MONITOR'S ACRONYM(S)	
				11. SPONSOR/MONITOR'S REPORT NUMBER(S)	
12. DISTRIBUTION/AVAILABILITY STATEMENT Approved for public release; distribution unlimited					
13. SUPPLEMENTARY NOTES					
14. ABSTRACT					
15. SUBJECT TERMS					
16. SECURITY CLASSIFICATION OF:			17. LIMITATION OF ABSTRACT	18. NUMBER OF PAGES	19a. NAME OF RESPONSIBLE PERSON
a. REPORT unclassified	b. ABSTRACT unclassified	c. THIS PAGE unclassified			

1 **The Kelvin wave and the Madden-Julian Oscillation in aqua-planet simulations by**
2 **the Naval Research Laboratory Spectral Element Atmospheric Model (NSEAM)**

3

4 Young-Joon Kim¹, Francis X. Giraldo², Maria Flatau¹, Chi-Sann Liou¹, and Melinda S.
5 Peng¹

6 ¹Naval Research Laboratory, Monterey, CA

7 ²Naval Postgraduate School, Monterey, CA

8 yj.kim@nrlmry.navy.mil

9

10 5 December 2007

11 *Submitted to Geophysical Research Letters*

12

13 The Naval Research Laboratory (NRL) Spectral Element Atmospheric Model (NSEAM)
14 with full physics included is used to investigate the organization and propagation of
15 equatorial waves under the aqua-planet conditions. The sensitivity of the simulation to
16 the distribution of the vertical levels and selected details of the model's precipitation
17 physics is discussed utilizing simulated convective precipitation with the aid of the time-
18 longitude plots and spectral diagrams. It is shown that the Kelvin wave simulation
19 depends strongly on the details of the vertical level distribution and the methods
20 associated with the lifting condensation level. While significant variability is found
21 among the aqua-planet simulations by global atmospheric models, the new model
22 captures the essential interaction between the dynamics and physics of the atmosphere
23 such that the simulated speed and spectrum of the eastward propagating Kelvin waves

1 and the signature of the Madden-Julian Oscillation are as approximately predicted by
2 simplified theory and limited observations.

3

4

5 **1. Introduction**

6

7 The US Navy has recently developed a new high-accuracy global atmospheric
8 model, which scales efficiently on current and future state-of-the-art computing
9 platforms: the Naval Research Laboratory (NRL) Spectral Element Atmospheric Model,
10 or NSEAM. Its dynamical core [*Giraldo and Rosmond, 2004*] is based on “spectral
11 element” methods projected to three-dimensional Cartesian coordinates, which
12 effectively eliminate the pole singularity problem of spherical coordinates and combine
13 the local domain decomposition property of finite-element methods with the high-order
14 accuracy of spectral transform methods.

15 NSEAM can adopt any horizontal model grid, fixed or variable, and various time
16 integrators such as Eulerian [*Giraldo and Rosmond, 2004*], semi-implicit [*Giraldo, 2005*],
17 semi-Lagrangian [*Giraldo et al., 2003*], or hybrid Eulerian-Lagrangian semi-implicit
18 [*Giraldo, 2006*] methods. Its spectral element formulation maintains the high-order
19 accuracy of spherical harmonics that the current Navy’s global atmospheric model is
20 based on, while it offers flexibility to use any form of variable grid to enhance horizontal
21 grid resolutions in strategic regions. Its dynamical core scales efficiently, i.e., allows the
22 use of large numbers of processors, and was validated using various barotropic and
23 baroclinic test cases [*Giraldo and Rosmond, 2004*]. The model can be discretized

1 vertically with any grid, but the mass and energy conserving flux-form of the finite-
2 difference method on the terrain-following (σ) coordinate is first selected for comparison
3 with existing models.

4 For this study, we modify and expand the NSEAM dynamical core to include the
5 physics package used in the operational version of the Navy Operational Global
6 Atmospheric Prediction System or NOGAPS (*Hogan and Rosmond* [1991]; see also *Kim*
7 [2007] for a list of recent model physics improvements), but without the land surface
8 parameterization. We select the hexahedral grid that consists of six faces of a
9 hexahedron, each of which contains a desired number of quadrilateral elements [*Giraldo*
10 *and Rosmond*, 2004]. The grid can be stretched to enhance the resolution of a selected
11 region, e.g., the tropics.

12 Among the methods to validate an atmospheric model is to force the model under
13 controlled and simplified sets of boundary and initial conditions so that the results can be
14 interpreted in a relatively straightforward manner and also inter-comparable to those of
15 other similar models although the correct solution is not quite known except by
16 simplified theory and limited indirect observations. A good recent example is the aqua-
17 planet experiments proposed by *Neale and Hoskins* [2001a, b] in which the earth is
18 covered with flat water only. These experiments provide a useful and convenient test-bed
19 for investigating the interaction between the dynamics and physics in atmospheric models.

20 In this study, we validate NSEAM by configuring it for aqua-planet experiments
21 following *Neale and Hoskins* [2001a]. We perform various sensitivity experiments in
22 order to improve the aqua-planet simulation. Sensitivity of aqua-planet simulations to
23 horizontal resolution was studied previously. For example, *Lorant and Royer* [2001]

1 found from general circulation model (GCM) experiments that with higher resolution the
2 convective cells are more intensified and concentrated, being accompanied by improved
3 simulation of equatorial waves that modulate near-equatorial convection. Sensitivity of
4 aqua-planet simulations to vertical resolution was also studied earlier. For example,
5 *Inness et al.* [2001] compared between 19 and 30 (unevenly-spaced) layer versions of
6 their GCM and discussed its implications for Madden-Julian Oscillation (MJO) in view
7 of the moisture budget. They reported that the effect of convection is to moisten / dry the
8 lower troposphere in their 19 / 30 layer simulations, respectively. In the present study,
9 we investigate further sensitivity of the aqua-planet simulations to selected details of the
10 model such as the vertical distribution – as well as the resolution - of the model levels
11 and the way the lifting condensation level (LCL) is calculated or used in the context of
12 the frequency and propagation of simulated Kelvin waves and MJO.

13

14

15 **2. The Aqua-Planet Experiments**

16

17 NSEAM is configured to perform aqua-planet simulations basically following the
18 Aqua-Planet Experiment (APE) Intercomparison Project recommendations [*Neale and*
19 *Hoskins, 2001a, b*]: The earth is covered with water with no orography, land or sea ice.
20 The sea surface temperature prescribed is zonally uniform and symmetric with respect to
21 the equator as in the “control” case of *Neale and Hoskins* [2001a] – see Fig. 1. Earth
22 eccentricity and obliquity are set to zero. The solar insolation is fixed to the equinoctial
23 condition with solar constant of 1365 Wm^{-2} . We include the diurnal cycle in this study.

1 CO₂ is prescribed to the amount of 348 ppmv following the Atmospheric Model
2 Intercomparison Project (AMIP; *Gates* [1992]) II. The ozone is also taken from AMIP II
3 and zonally averaged, but is symmetrized with respect to the equator for this study.
4 Furthermore, we take the year 2005 averages of humidity and air temperature from the
5 National Centers for Environmental Prediction / National Center for Atmospheric
6 Research (NCEP/NCAR) Reanalysis data, which are also zonally-averaged and
7 symmetrized with respect to the equator. We impose this latitudinal symmetry of the
8 ozone, humidity and air temperature to remove the initial asymmetry so that any
9 asymmetry that develops during simulation is due solely to the model physics.

10 The time integration is done semi-implicitly with second-order backward
11 difference method. The time step is 300 s while the radiation parameterization is called
12 every hour. We include a simple second-order hyper-viscosity for physics by
13 generalizing the approach introduced in *Giraldo* [1999] with $\frac{\partial q}{\partial t} = S(q) + \mu \nabla^2 q$, where q is
14 any prognostic physical variable, S represents the forcing, and $\mu = 1 \times 10^6$ (m²s⁻¹) is the
15 default value used in this study. For the horizontal grid, we choose 6 elements on one
16 face in one direction and 8th polynomial order of the basis functions (Fig.1). This
17 horizontal resolution is roughly equivalent to the triangular spectral truncation at
18 wavenumber 54 (i.e., T54) or 2.2°. We use 20 or 30 vertical levels, either evenly-spaced
19 or unevenly-spaced in σ with the model top pressure of 1 hPa (Fig. 2). The simulations
20 are run for one year with the first 30 days considered a spin-up period and excluded in the
21 averages of 12-hour interval outputs.

22

23

3. The Simulation of Kelvin Waves and Madden-Julian Oscillation

Figure 3 shows time-longitude (or Hovmoeller) plots of the convective precipitation averaged over the equator ($5^{\circ}\text{S} \sim 5^{\circ}\text{N}$) from simulation day 30 to 120. We found that after about 20 days, the simulations become very steady (at least for two years) and selected this 90-day interval to be compared with Fig. 3a of *Neale and Hoskins* [2001b]. There is clear difference between L20 (Fig. 3a) and L30 (Fig. 3b) evenly-spaced vertical level cases (L20e and L30e, hereafter) in the speed of the eastward-propagating waves (i.e., Kelvin waves) while the magnitude of the precipitation is similar. With L20e it takes about slightly more than two months in average for the Kelvin waves to circle the earth along the equator, but with L30e it takes more than four months. This speed difference can be explained by the greater vertical scale of the convective systems in the L20e case, which implies greater equivalent depth and higher vertical modes generated in this case. The vertical scale for both cases was estimated from the average cloud-top height, which was about twice higher in L20e than in L30e.

The propagation speeds of Kelvin waves in both L20e and L30e are fairly low compared with the observed atmospheric Kelvin waves (e.g., *Masunaga et al.* [2006]) and other simulations (e.g., *Neale and Hoskins* [2001b], *Moncrieff et al.* [2007]). However, changing the vertical structure of the model strongly influences the phase speed of the modeled waves. Figure 3c shows the Hovmoeller diagram for L30u (L30 with unevenly-spaced levels), with tightly spaced levels near the surface and at the top of the atmosphere and loosely spaced levels in between (compare Figs. 2b and 2c). The

1 Kelvin wave propagation speed for L30u is higher than those for L30e and L20e and
2 closer to the observed values.

3 The corresponding convective precipitation, averaged over about 11 months (days
4 30~365), reveals relatively narrow / broad and strong / weak distribution along the
5 equatorial band with L30e / L30u case, respectively (implicitly shown in Figs. 3b and 3c;
6 note the difference in the color scale). In order to understand this difference, we
7 computed the difference of the moisture between these two cases and found the moisture
8 over the equator in the lower troposphere (averaged over 700 ~ 950 hPa) was greater with
9 L30u, implying that more moisture is available for L30u with the vertical intervals in this
10 height range larger than L30e ($\sigma \sim 0.93$ corresponds to 940 hPa; see Fig. 2).

11 We then compared the zonally averaged cumulus heating rate (also averaged over
12 700 ~ 950 hPa for days 30~365) between L30e and L30u, which is derived from the
13 temperature tendency calculated by the Emanuel convective cloud parameterization used
14 in our model [*Emanuel and Zivkovic-Rothman, 1999; Peng et al., 2004*]. There was a
15 marked difference between the two cases; L30e showed the highest peak directly over the
16 equator and secondary peaks over the middle latitudes whereas L30u showed the highest
17 peaks over the middle latitudes and the sharp secondary peak over the equator. It turned
18 out (not shown) that in L30e the moisture (although itself is less abundant) is more
19 localized over the equator, the easterly winds are stronger over the equator and the
20 meridional winds are stronger toward the equator, resulting in stronger and more
21 localized low-level moisture convergence toward the equator and, consequently, stronger
22 and more localized moisture convection and convective precipitation.

1 The spectral analysis of tropical waves introduced by *Wheeler and Kiladis* [1999]
2 is an effective and convenient tool for investigating the organization and propagation of
3 equatorial waves. Figure 4 compares the (equator-) symmetric component of the
4 wavenumber-frequency decomposition divided by the background spectrum obtained
5 using the simulated convective precipitation. The excessively low propagation speeds of
6 L20e and L30e shown by the Hovmoeller plots (Figs. 3a, 3b) are confirmed in Figs. 4a
7 and 4b whereas L30u (Fig. 4c) reveals much improved frequency compared with the
8 theoretical lines obtained from the dispersion relations for a shallow water system (see
9 the Fig. 4 legend for details).

10 Moreover, we find that the Kelvin wave propagation depends critically on details
11 of the model physics; particularly those that involve vertical motion. First, we modify the
12 Emanuel convective parameterization so that that a thicker layer is used to determine the
13 LCL. The Hovmoeller plot from this experiment with L30u is shown in Fig. 3d. The
14 rather scattered cloud clusters that were present in L30u with the old LCL formulation
15 (Fig. 3c) are now better organized with the new LCL formulation (Fig. 3d) while
16 maintaining the dominant propagation speed of the old LCL case (Fig. 3c). Next, we
17 change the limiting value of the specified temperature deficit at the LCL (ΔT_{\max}) in the
18 Emanuel convective cloud parameterization from 0.9 to 1.2 K, which then enhances
19 chance of the convection. The result (Fig. 3e) involves far stronger organization of the
20 cloud clusters. It is interesting that increasing ΔT_{\max} produces the bimodal structure of
21 the eastward propagating perturbations with the slow moving waves propagating with the
22 speed of MJO (marked by dashed lines) and faster waves corresponding to observed
23 Kelvin waves (solid lines). When the precipitation fields are filtered for the observed

1 MJO and Kelvin wave modes, we can see the resemblance between the modified ΔT_{\max}
2 case and observed Kelvin and MJO modes, with more intense Kelvin waves developing
3 during the “wet” MJO phase. This relationship is not present in other experiments
4 presented in this study.

5 The Wheeler-Kiladis diagrams corresponding to these additional experiments are
6 presented in Figs. 4d and 4e. It is apparent that with these physics modifications the
7 wave spectrum patterns deviate more from the linear solutions (the theoretical lines) than
8 the original case (Fig. 4c). It is perhaps due to a separation of the wave modes from pure
9 Kelvin wave mode to a faster moving Kelvin wave mode and a slower moving mode.
10 This is clearly seen as separated spectral peaks in Fig. 4e and additionally in Fig. 4f that
11 is from another experiment with both the new LCL and ΔT_{\max} . The spectral peaks with
12 periods greater than 30 days at eastward propagating wave numbers 1 and 2 are
13 considered a signature of the MJO [*Neale and Hoskins, 2001b*]. Our spectrum (Fig. 4f, in
14 particular) is fairly similar to that based on observed deep-storm cloudiness and rainfall
15 (see Fig. 1e of *Masunaga et al. [2006]* and Fig. 10d of *Cho et al. [2004]*, respectively).
16 In this regard, the slower moving mode, which is represented by the slower moving
17 clusters (Figs. 3d, 3e) and the low frequency spectral peak (Figs. 4c, 4e, 4f), may be
18 associated with the MJO. On the other hand, the spectral peak that appears at wave
19 number 5 in Fig. 4d, which is also found in Fig. 3b of *Neale and Hoskins [2001b]*,
20 requires further investigation.

21

22

23 **4. Concluding Remarks**

1

2 Even under a controlled environment of the aqua-planet experiments, the
3 propagation of equatorial waves vary widely among the models – even the simulated
4 propagation directions of the equatorial waves are opposite in some models (see, e.g., Fig.
5 3 of *Moncrieff et al.* [2007]). This can be due to many reasons, but the convective cloud
6 parameterization may be the prime suspect. Atmospheric models are sensitive to many
7 details of the model, in particular to the physical parameterizations involving vertical
8 motions of air parcels. Indeed, cumulus parameterization is considered one of the most
9 dominant modeling components that generate uncertainties in large-scale atmospheric
10 simulation (e.g., *Tomita et al.* [2005], *Moncrieff et al.* [2007]).

11 In this study we have explored such uncertainties utilizing our model, NSEAM.
12 We have demonstrated that the simulations of convective activities can be quite different
13 even with the same convective cloud parameterization depending on the distribution of
14 vertical levels as well as they are sensitive to the details of the parameterization itself.
15 For this reason, some standardization of vertical levels may be useful for more direct
16 intercomparison among the models (e.g., for the APE). Furthermore, we have presented
17 results demonstrating that the model can be calibrated to capture some basic
18 characteristics of the Kelvin waves and MJO, which is encouraging considering the wide
19 variability found among similar aqua-planet simulations.

20

21

22 **Acknowledgments**

23

1 The support from the sponsor, the Office of Naval Research under ONR Program
2 Elements 0602435N and 0601153N is acknowledged. The comments from R. Hodur, S.
3 Chang, and discussion with T. Hogan are appreciated. The computing time was provided
4 jointly by the Naval Research Laboratory, Monterey, and the DoD NAVO MSRC (Naval
5 Oceanographic Office Major Shared Resource Center) via the HPC program.

6

7

8 **References**

9

- 10 Cho, H. -K., K. P. Bowman, and G. R. North (2004), Equatorial waves including the
11 Madden-Julian Oscillation in TRMM rainfall and OLR data. *J. Climate* 17, 4387-
12 4406.
- 13 Emanuel, K. A., and M. Zivkovic-Rothman (1999), Development and evaluation of a
14 convection scheme for use in climate models, *J. Atmos. Sci.* 56, 1766-1782.
- 15 Gates, W. L. (1992), AMIP: The Atmospheric Model Intercomparison Project. *Bull.*
16 *Amer. Meteorol. Soc.* 73, 1962-1970.
- 17 Giraldo, F. X. (1999), Trajectory calculations for spherical geodesic grids in Cartesian
18 space. *Mon. Wea. Rev.* 127, 1651-1662.
- 19 Giraldo, F. X. (2005), Semi-implicit time-integrators for a scalable spectral element
20 atmospheric model. *Q. J. R. Meteorol. Soc.* 131, 2431-2454. doi: 10.1256/qj.03.218
- 21 Giraldo, F. X. (2006), Hybrid Eulerian-Lagrangian semi-implicit time-integrators.
22 *Computers and Mathematics with Applications.* 52, 1325-1342.

1 Giraldo, F. X., J. B. Perot, and P. F. Fischer (2003), A spectral element semi-Lagrangian
2 (SESL) method for the spherical shallow water equations. *J. Comput. Phys.* *190*,
3 623-650.

4 Giraldo, F. X., and T. E. Rosmond (2004), A scalable spectral element Eulerian
5 atmospheric model (SEE-AM) for NWP: Dynamical core tests. *Mon. Wea. Rev.* *132*,
6 133-153.

7 Hogan, T. F., and T. E. Rosmond (1991), The description of the Navy Operational Global
8 Atmospheric Prediction System's spectral forecast model, *Mon. Wea. Rev.* *119*,
9 1186-1815.

10 Inness, P. M., J. M. Slingo, S. J. Woolnough, R. B. Neale, and V. D. Pope (2001),
11 Organization of tropical convection in a GCM with varying vertical resolution;
12 implications for the simulation of the Madden-Julian Oscillation, *Clim. Dyn.* *17*,
13 777-793.

14 Kim, Y. -J. (2007), Balance of drag between the middle and lower atmospheres in a
15 global atmospheric forecast model, *J. Geophys. Res.*, *112*, D13104,
16 doi:10.1029/2007JD008647.

17 Lorant, V., and J. -F. Royer (2001), Sensitivity of equatorial convection to horizontal
18 resolution in aqua-planet simulations with a variable-resolution GCM. *Mon. Wea.*
19 *Rev.* *129*, 2730-2745.

20 Masunaga, H., T. S. L'Ecuyer, and C. D. Kummerow (2006), The Madden-Julian
21 Oscillation recorded in early observations from the Tropical Rainfall Measuring
22 Mission (TRMM). *J. Atmos. Sci.* *63*, 2777-2794.

1 Moncrieff, M., M. A. Shapiro, J. M. Slingo, and F. Molteni (2007), Collaborative
2 research at the intersection of weather and climate. *WMO Bulletin*. 56 (3).

3 Neale, R. B., and B. J. Hoskins (2001a), A standard test for AGCMs and their physical
4 parameterizations. I: The proposal. *Atmos. Sci. Letters*. 1,
5 doi:10.1006/asle.2000.0019.

6 Neale, R. B., and B. J. Hoskins (2001b), A standard test for AGCMs and their physical
7 parameterizations. II: Results for the Met Office model. *Atmos. Sci. Letters*. 1,
8 doi:10.1006/asle.2000.0020.

9 Peng, M. S., J. A. Ridout, and T. F. Hogan (2004), Recent modifications of the Emanuel
10 convective scheme in the Naval Operational Global Atmospheric Prediction System.
11 *Mon. Wea. Rev.* 132, 1254-1268.

12 Tomita, H., H. Miura, S. Iga, T. Nasuno, and M. Satoh (2005), A global cloud-resolving
13 simulation: Preliminary results from an aqua planet experiment, *Geophys. Res. Lett.*,
14 32, L08805, doi:10.1029/2005GL022459.

15 Wheeler, M., and G. N., Kiladis (1999), Convectively coupled equatorial waves: analysis
16 of clouds and temperature in the wavenumber-frequency domain. *J. Atmos. Sci.* 56,
17 374–399.

18
19

20 **Figure Captions**

21

22 Fig. 1. The sea surface temperature [K] prescribed for the aqua-planet experiments with
23 NSEAM, proposed by *Neale and Hoskins* [2001a]. Superimposed are the hexahedral grid

1 points with 6 elements on one face in one direction and 8th polynomial order of the basis
2 functions.

3

4 Fig. 2. The vertical grids used for the NSEAM aqua-planet simulations. (a) 20 evenly-
5 spaced σ levels, (b) 30 evenly-spaced σ levels, and (c) 30 unevenly-spaced σ levels with
6 tightly-spaced levels near the surface and the top and loosely-spaced intermediate levels.

7

8 Fig. 3. Time-longitude plot from days 30 to 120 of the convective precipitation [10-
9 mm/day] averaged for an equatorial band ($5^{\circ}\text{S} \sim 5^{\circ}\text{N}$) from the NSEAM aqua-planet
10 experiments (a) L20e, (b) L30e, (c) L30u, (d) L30u with new LCL, and (e) L30u with
11 modified ΔT_{max} . Note that a smaller contour interval is used for (c) ~ (e). The solid lines
12 are drawn to help estimate the propagation speed of cloud clusters. The dashed lines in
13 (d) and (e) are drawn to identify slower moving clusters distinguished from faster moving
14 counterparts denoted by the solid lines.

15

16 Fig. 4. The symmetric component of the wavenumber-frequency decomposition of the
17 convective precipitation following *Wheeler and Kiladis* [1999] for cases (a) L20e, (b)
18 L30e, (c) L30u, (d) L30u with new LCL, (e) L30u with modified ΔT_{max} , and (f) L30u
19 with both new LCL and modified ΔT_{max} for days 30 through 365. The straight lines
20 denote the shallow-water dispersion relations for equatorial Kelvin waves as shown in
21 Fig. 3b of *Neale and Hoskins* [2001b]. Also shown in (a) are the approximate Kelvin
22 wave propagation speeds, which correspond to equivalent depths of 50, 25 and 12 m from
23 left.

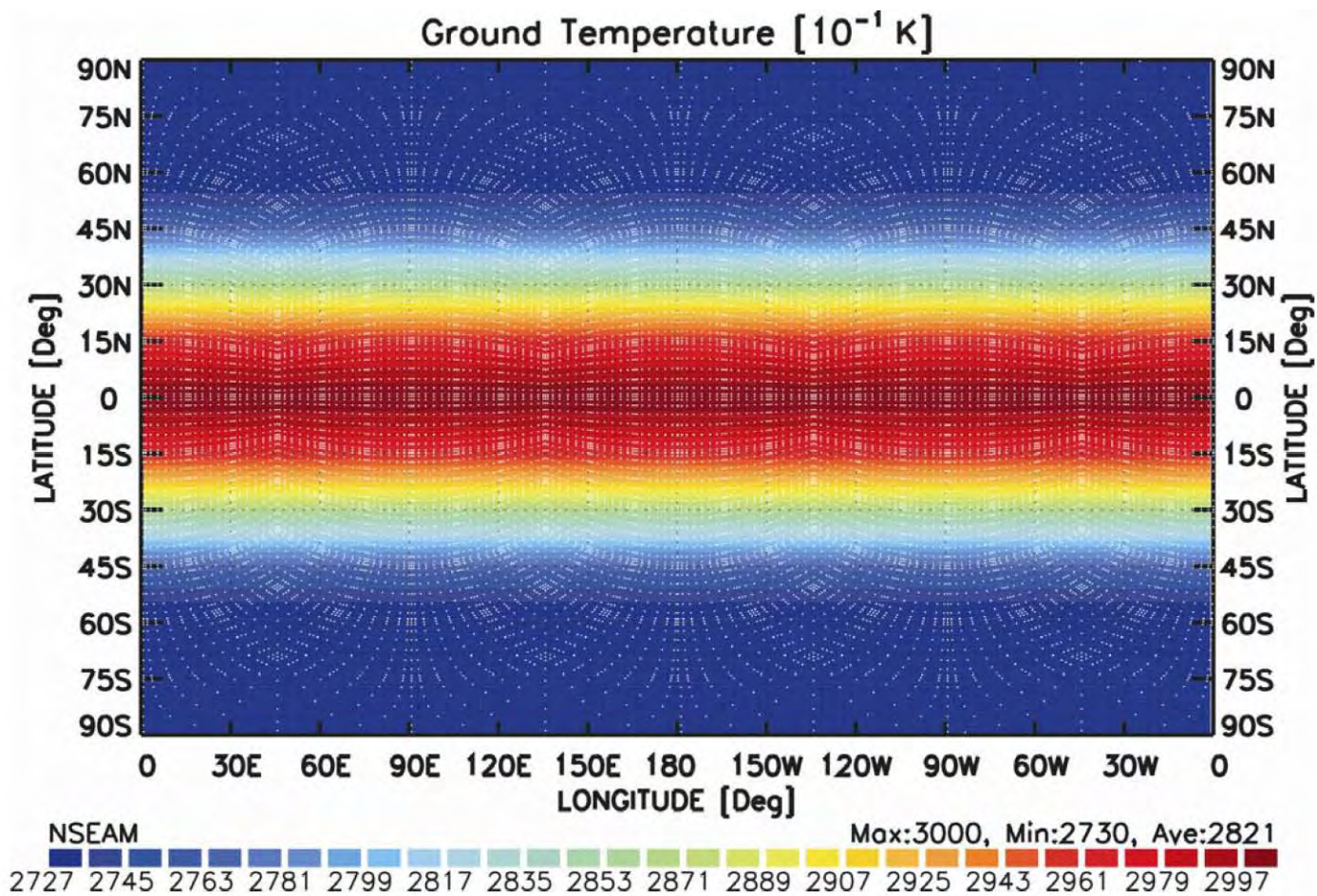


Figure 1

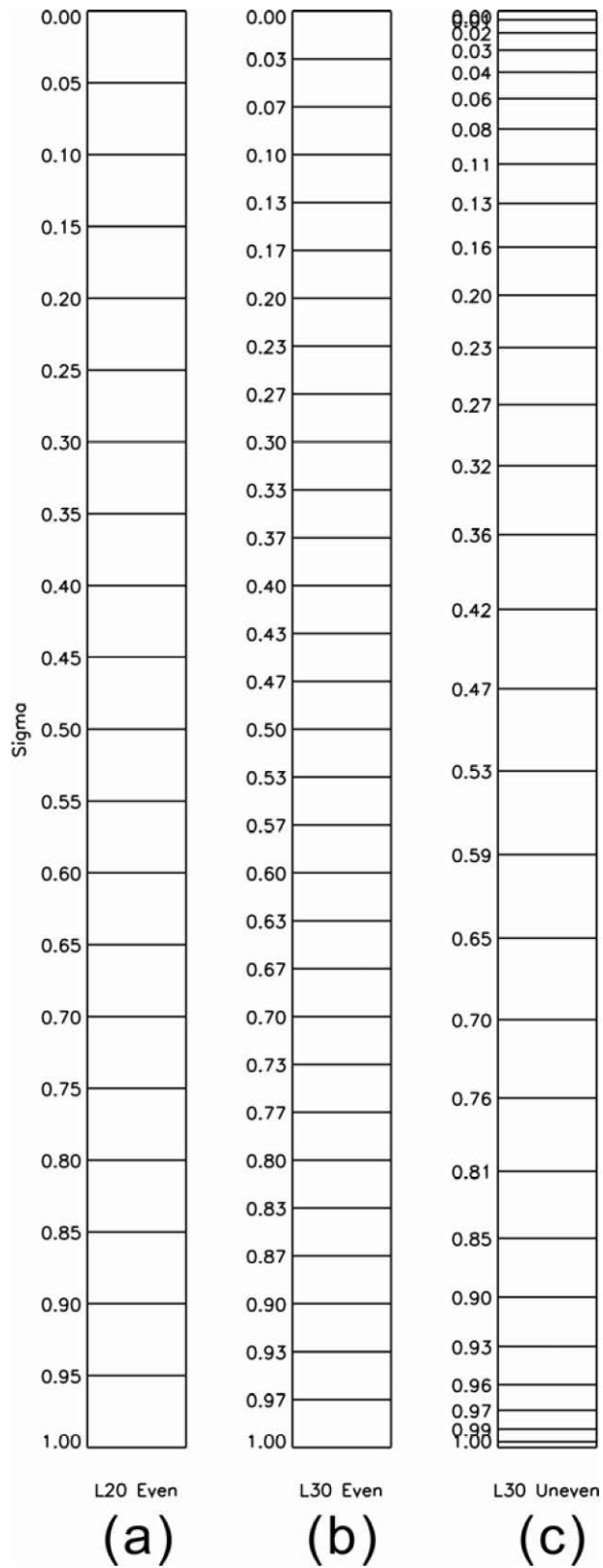


Figure 2

Convective Precipitation (5S-5N) [10^{-1} mm/day]

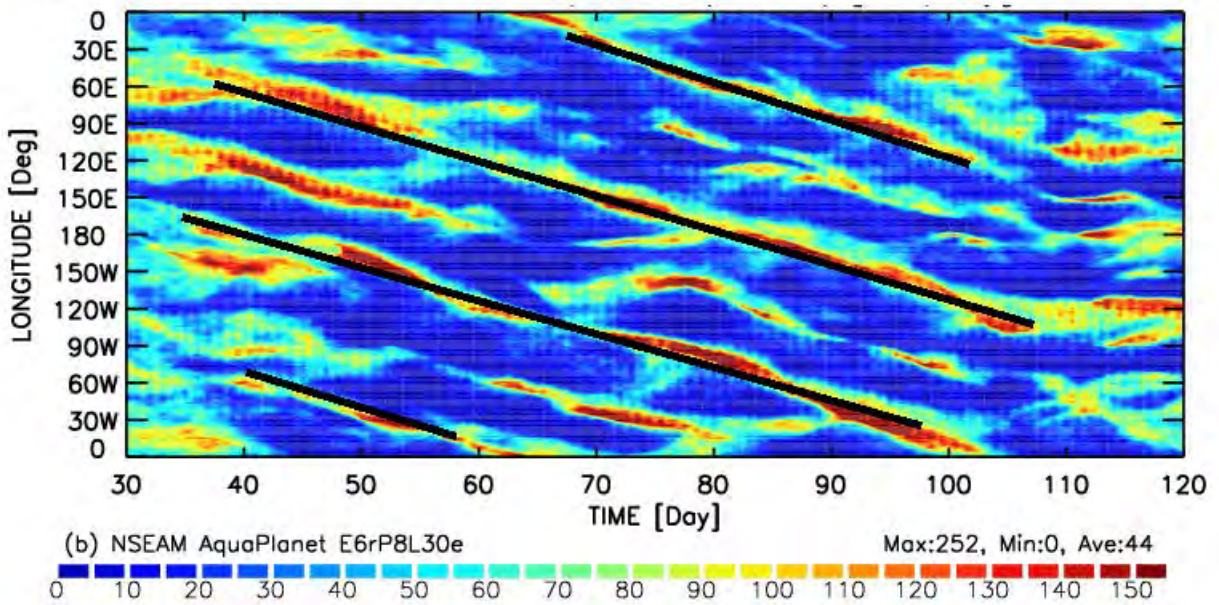
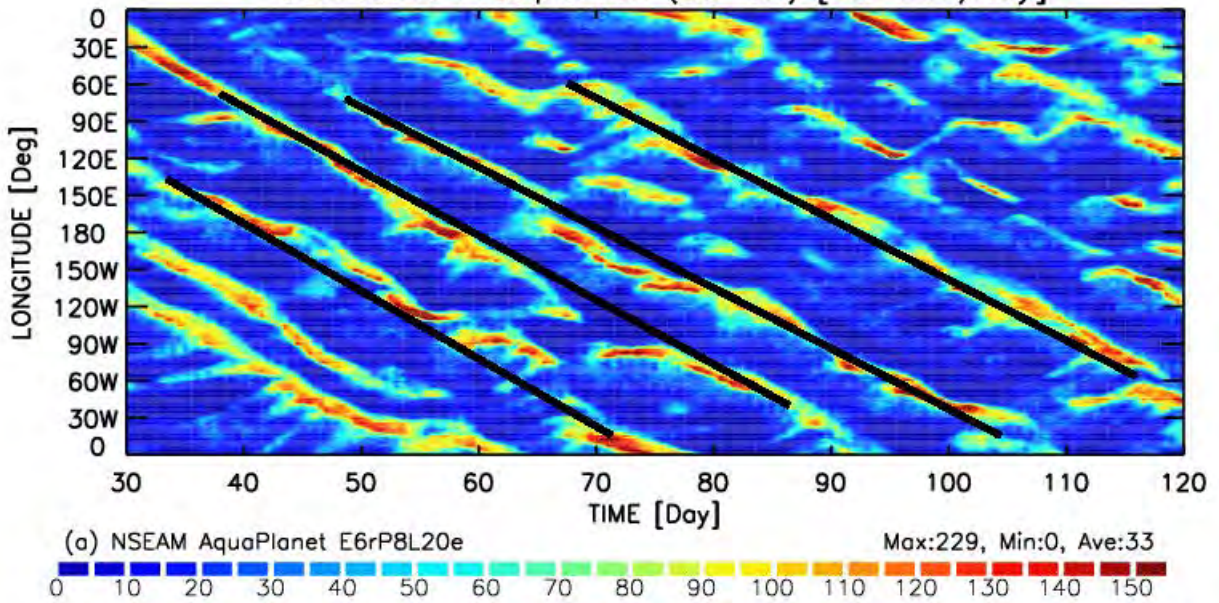


Figure 3

Convective Precipitation (5S–5N) [10^{-1} mm/day]

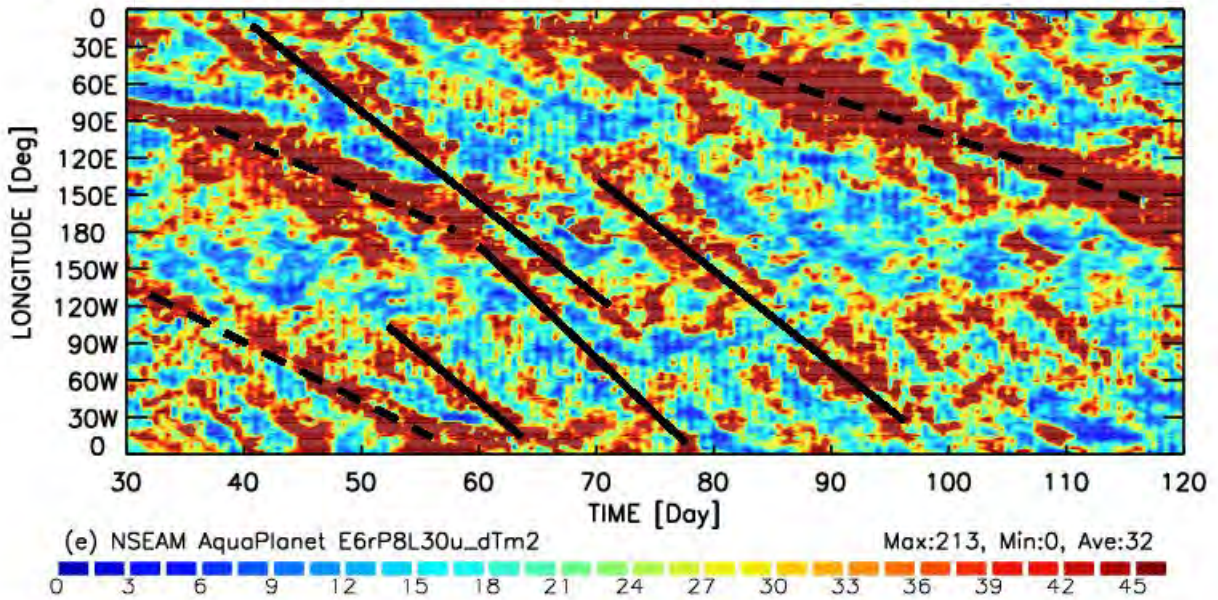
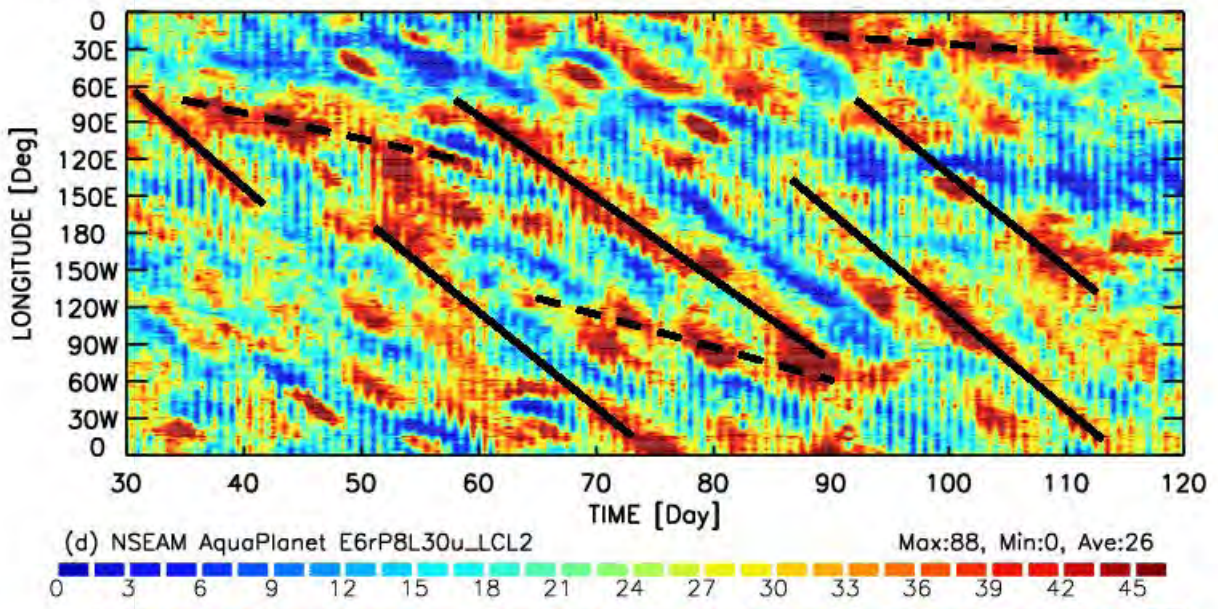
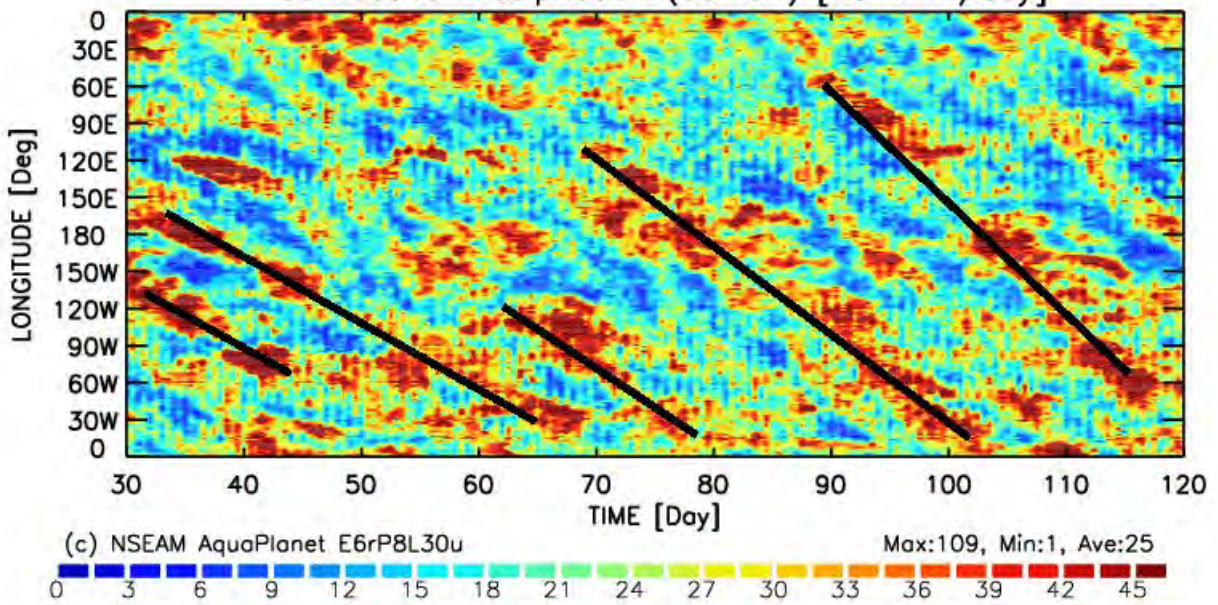


Figure 3 (cont.)

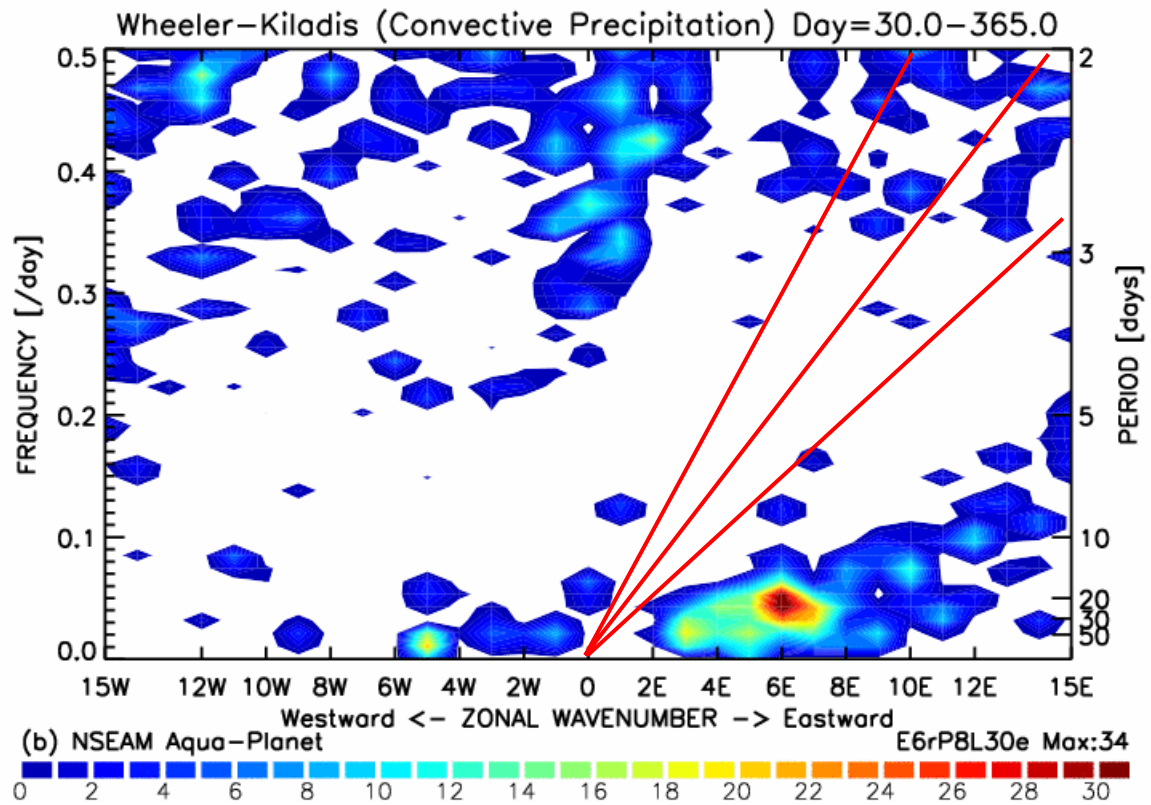
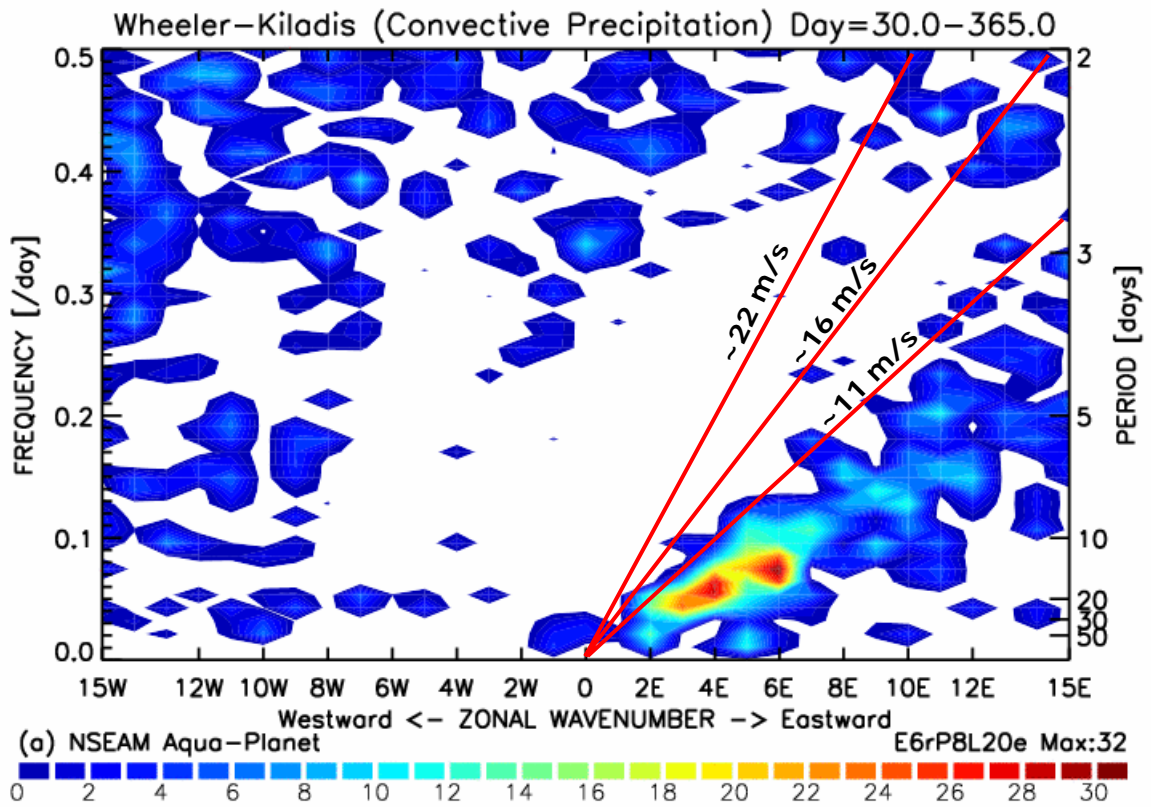


Figure 4

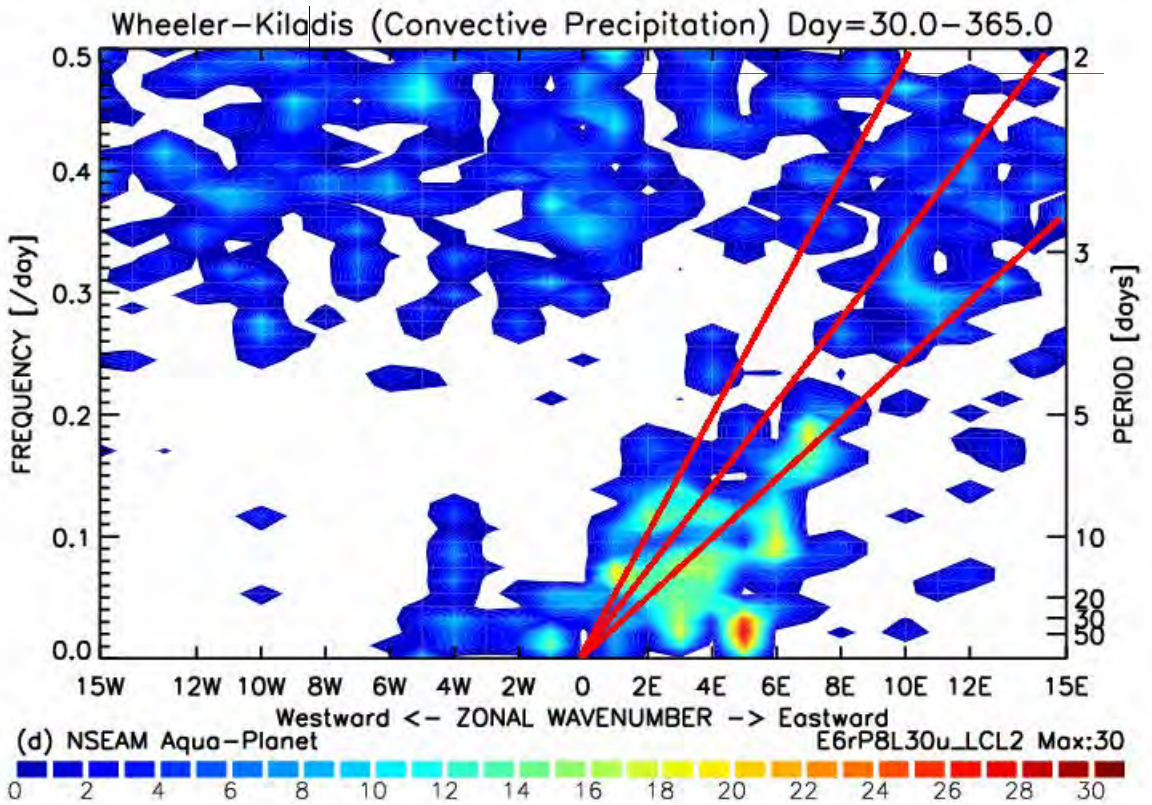
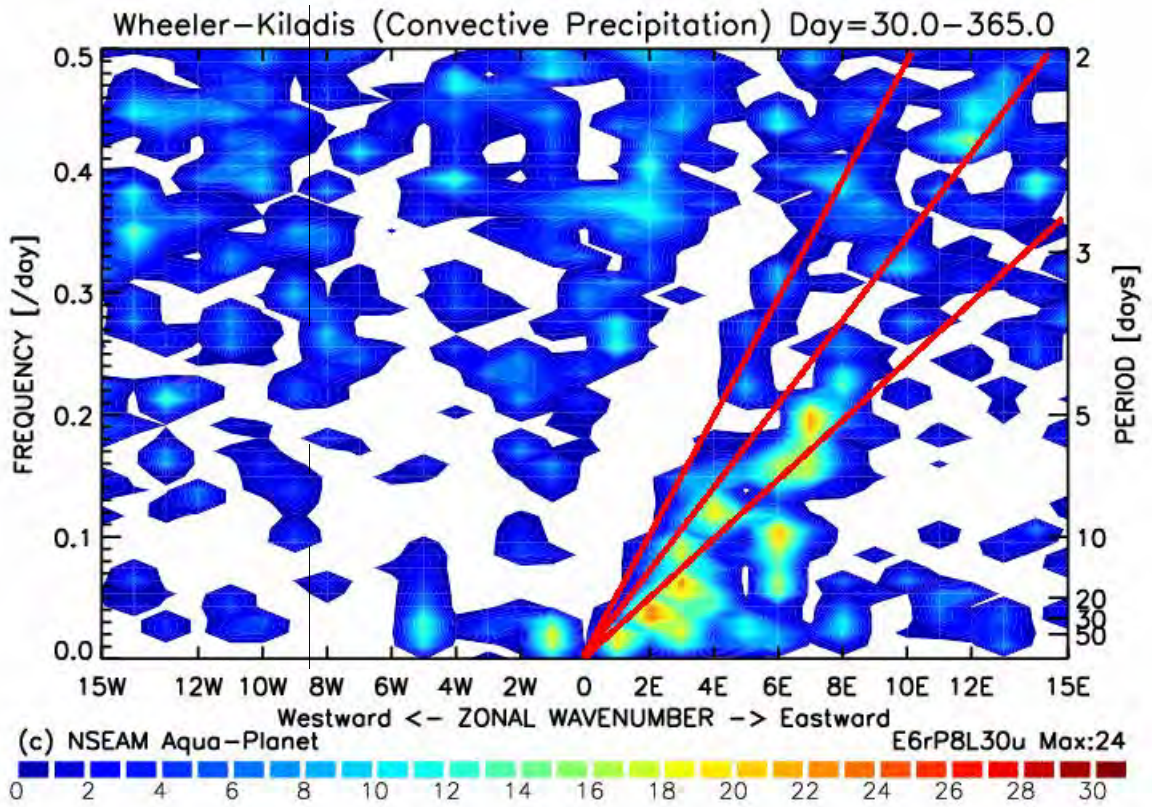


Figure 4 (cont.)

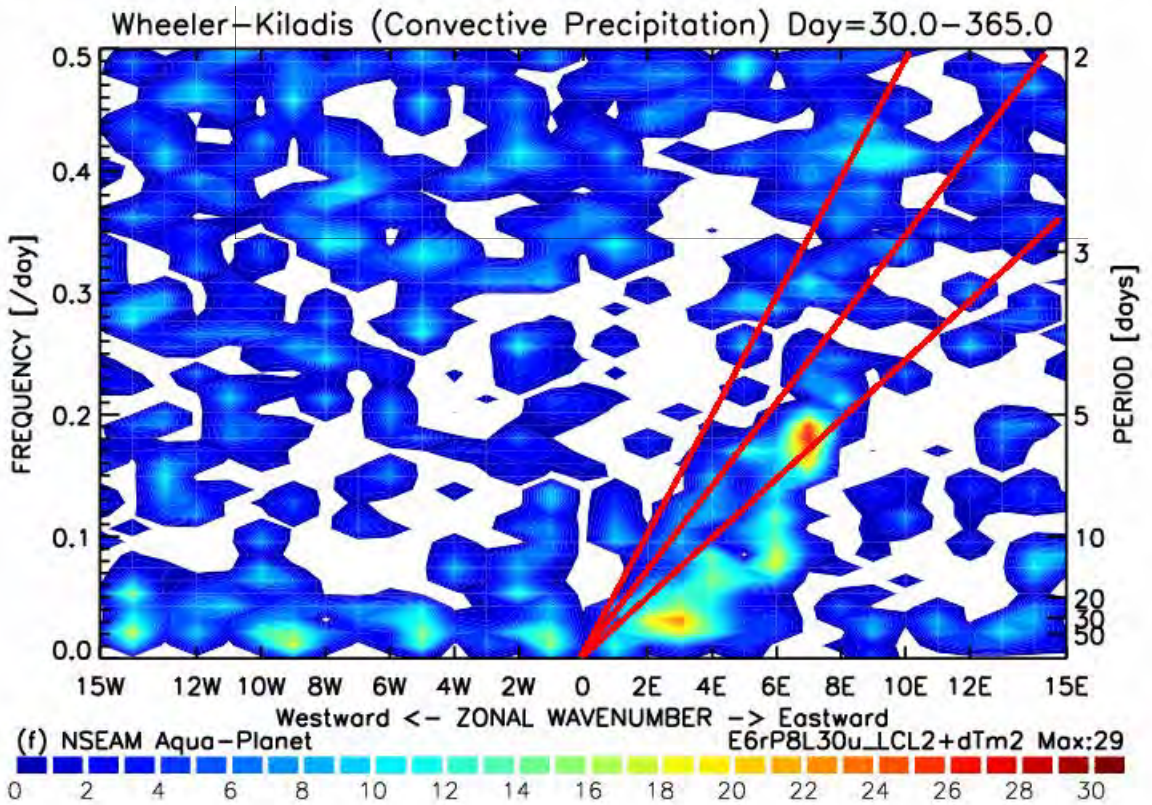
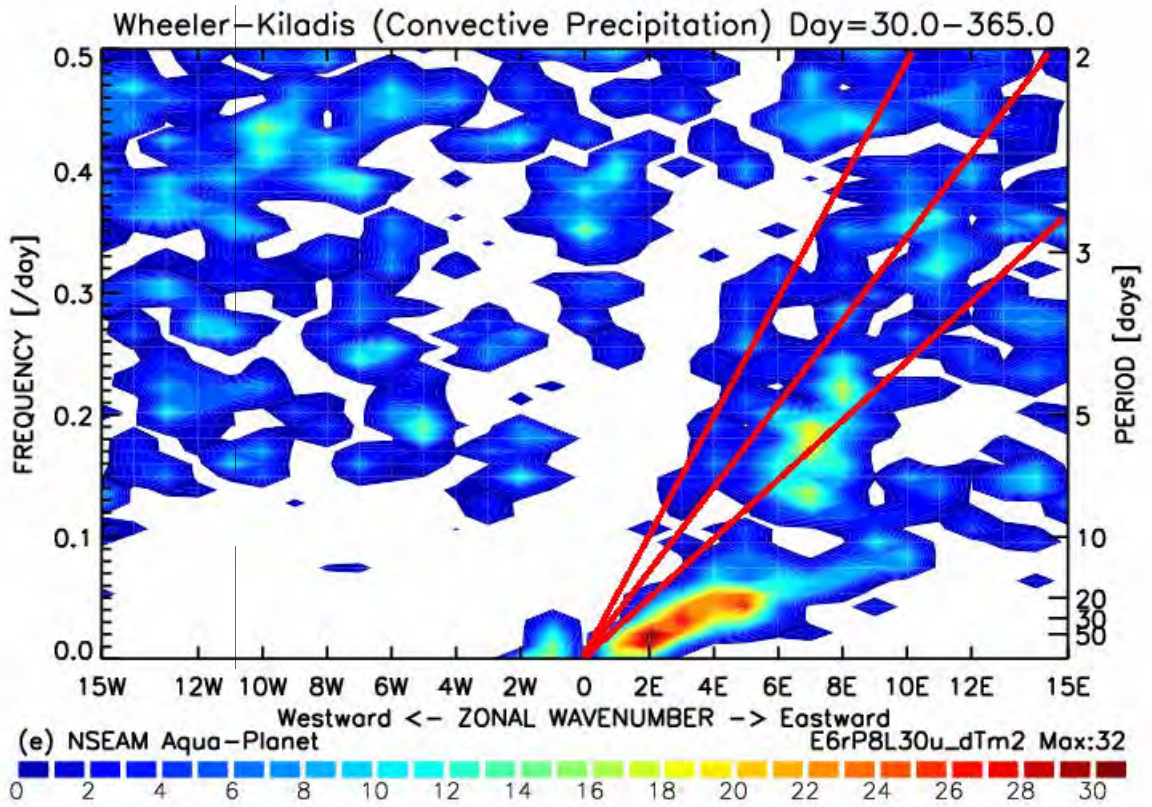


Figure 4 (cont.)